Bioactive Materials 6 (2021) 3839–3850

Contents lists available at ScienceDirect

Bioactive Materials

journal homepage: www.sciencedirect.com/journal/bioactive-materials

Mn-containing bioceramics inhibit osteoclastogenesis and promote osteoporotic bone regeneration via scavenging ROS

Jianmei Li [a,1], Cuijun Deng [b,1], Wanyuan Liang [a], Fei Kang [a], Yun Bai [a], Bing Ma [b], Chengtie Wu [b,**], Shiwu Dong [a,c,*]

[a] Department of Biomedical Materials Science, School of Biomedical Engineering, Third Military Medical University (Army Medical University), Chongqing, 400038, China

[b] State Key Laboratory of High Performance Ceramics and Superfine Microstructure, Shanghai Institute of Ceramics, Chinese Academy of Sciences, Shanghai, 200050, China

[c] State Key Laboratory of Trauma, Burns, and Combined Injury, Third Military Medical University (Army Medical University), Chongqing, 400038, China

ARTICLE INFO

Keywords:
Mn-containing bioceramics
Antioxidant biomaterials
Osteoclastogenesis
ROS
Osteoporotic bone regeneration

ABSTRACT

Osteoporosis is caused by an osteoclast activation mechanism. People suffering from osteoporosis are prone to bone defects. Increasing evidence indicates that scavenging reactive oxygen species (ROS) can inhibit receptor activator of nuclear factor κB ligand (RANKL)-induced osteoclastogenesis and suppress ovariectomy-induced osteoporosis. It is critical to develop biomaterials with antioxidant properties to modulate osteoclast activity for treating osteoporotic bone defects. Previous studies have shown that manganese (Mn) can improve bone regeneration, and Mn supplementation may treat osteoporosis. However, the effect of Mn on osteoclasts and the role of Mn in osteoporotic bone defects remain unclear. In present research, a model bioceramic, Mn-contained β-tricalcium phosphate (Mn-TCP) was prepared by introducing Mn into β-TCP. The introduction of Mn into β-TCP significantly improved the scavenging of oxygen radicals and nitrogen radicals, demonstrating that Mn-TCP bioceramics might have antioxidant properties. The *in vitro* and *in vivo* findings revealed that Mn^{2+} ions released from Mn-TCP bioceramics could distinctly inhibit the formation and function of osteoclasts, promote the differentiation of osteoblasts, and accelerate bone regeneration under osteoporotic conditions *in vivo*. Mechanistically, Mn-TCP bioceramics inhibited osteoclastogenesis and promoted the regeneration of osteoporotic bone defects by scavenging ROS via Nrf2 activation. These results suggest that Mn-containing bioceramics with osteoconductivity, ROS scavenging and bone resorption inhibition abilities may be an ideal biomaterial for the treatment of osteoporotic bone defect.

1. Introduction

Osteoporosis is a global health problem that is characterized by severe bone loss and increased bone fragility. Postmenopausal osteoporosis has the largest number of patients. Approximately 50% of 65-year-old postmenopausal Caucasian or Asian women have osteoporosis [1,2]. Dysregulation of osteoclastogenesis is the main cause of osteoporosis [3,4]. Enhanced osteoclastogenesis due to oestrogen deficiency is the most notable characteristic of postmenopausal osteoporosis, leading to increased fragility, fractures and bone defects in postmenopausal women or oestrogen-depleted women [5]. Osteoclasts (OCs) are bone-specific multinucleated cells that are the main effectors of bone resorption and are indispensable in bone reconstruction, repair and the maintenance of mineral homeostasis [6]. Under osteoporotic conditions, excessive osteoclast activity induces drastically delayed healing of bone defects [7]. Thus, it is critical to develop biomaterials for treating osteoporotic bone defects though regulating osteoclast activity.

Reactive oxygen species (ROS) participates in bone homeostasis and

Peer review under responsibility of KeAi Communications Co., Ltd.

* Corresponding author. Department of Biomedical Materials Science, School of Biomedical Engineering, Third Military Medical University (Army Medical University), Chongqing, 400038, China.

** Corresponding author.

E-mail addresses: chengtiewu@mail.sic.ac.cn (C. Wu), dongshiwu@tmmu.edu.cn (S. Dong).

[1] Co-first author.

https://doi.org/10.1016/j.bioactmat.2021.03.039

Received 12 December 2020; Received in revised form 26 March 2021; Accepted 26 March 2021

bone remodelling via promoting bone resorption [8]. Increasing antioxidant defenses can prevent oestrogen deficiency-induced osteoporosis [9]. Receptor activator of nuclear factor κB ligand (RANKL) is an important cytokine that regulates OC differentiation and survival [10]. Increasing evidence indicates that ROS play key roles during RANKL-induced osteoclast formation and bone resorption [11]. Oestrogen deficiency induces ROS accumulation, promotes RANKL-mediated osteoclastogenesis and further promotes osteoclastic bone resorption [8,12]. Scavenging ROS can inhibit RANKL-induced osteoclastogenesis and suppress ovariectomy-induced osteoporosis [11,13,14]. Therefore, developing biomaterials with antioxidant properties to modulate osteoclast formation and function may be a treatment for osteoporotic bone defects.

As a bioresorbable ceramic with the characteristics of biocompatibility, degradability, and osteoconductive and osteoinductive, β-tricalcium phosphate (β-TCP) is widely used for bone tissue repair and regeneration [15]. However, under osteoporotic conditions, excessive activation of osteoclasts induces bone destruction and bone mass loss, resulting in loosening and displacement of implant materials, further affecting the process of bone defect repair [16]. Hence, the regeneration of osteoporotic bone defects with traditional β-TCP faces difficulties and challenges. It is well known that scaffolds with a beneficial ion microenvironment are conducive to tissue regeneration [17–19]. Mn is a trace element with an average concentration in bone of 1.7–3 ppm that is necessary for protein synthesis in bone tissues [20–22]. It has been reported that Mn^{2+} ions benefit osteoblast adhesion, viability, and proliferation by activating integrin [23,24]. Furthermore, increased osteogenic gene expression and a high collagen deposition rate were observed in multifunctional materials containing Mn^{2+} ions [25,26]. Recently, Mn^{2+} ions have been considered to be a means to improve bone regeneration due to their ability to promote osteogenic differentiation and maintain bone mass [27,28]. In addition, Mn supplementation in ovariectomized rats increases bone density and bone formation and inhibits bone loss, suggesting that Mn supplementation may be a treatment for osteoporosis [29,30]. Moreover, it has been reported that an appropriate amount of Mn^{2+} ions can significantly increase the levels of superoxide dismutase and peroxidase in tomato seedlings [31]. However, the exact mechanism of Mn in osteoporosis is unclear. The antioxidant properties of Mn and Mn-containing biomaterials remain unclear. The effects of Mn-containing biomaterials on OCs and their role in osteoporotic bone defects also remain unclear.

In present research, Mn-contained β-TCP (Mn-TCP) bioceramics were prepared by introducing Mn into β-TCP. We found that incorporated Mn into β-TCP could significantly improve the scavenging of oxygen radicals and nitrogen radicals. The results demonstrated that Mn-TCP bioceramics might have potential antioxidant properties. Given the critical role of ROS in osteoclast activity and oestrogen deficiency-induced osteoporosis and the potential antioxidant activity and osteogenic capacity of Mn-TCP bioceramics, we hypothesized that Mn-TCP bioceramics could inhibit osteoclast activity and promote osteoporotic bone defect regeneration. In this study, we assessed the effect of Mn-TCP bioceramics on RANKL-induced osteoclastogenesis *in vitro* and ovariectomized (OVX)-induced osteoporosis bone defect regeneration in rats *in vivo*, as well as the free radical scavenging capacity of Mn-TCP bioceramics and the underlying mechanisms. Our study may provide a novel therapeutic strategy for treating osteoporotic bone defects.

2. Materials

2.1. Synthesis of Mn-TCP and TCP powders

Pure TCP and Mn-TCP bioceramic powders were prepared via a coprecipitation method. Briefly, 103.8 g of $Ca(NO_3)_2{\cdot}4H_2O$ (Sinopharm Chemical Reagent, Shanghai, China) and 9.6 g of $MnCl_2{\cdot}4H_2O$ (Sigma, Merck, USA) were added into 965 mL of ultra-pure water (UPW) to prepare a Ca–Mn solution. And 43 g of $(NH_4)_2HPO_4$ (Sinopharm Chemical Reagent, Shanghai, China) was added into 650 mL of UPW to obtain a phosphate solution. And then we add the Ca–Mn solution into the phosphate solution (PH = 7.49–7.53) drop by drop. After 24 h of stirring, samples were experienced vacuum filtration and dried at 100 °C in a drying oven. After ball-milling for 3 h, the original Mn-TCP powder was sintered at 800 °C for another 3 h. Pure TCP bioceramic powder was synthesized in the same way without $MnCl_2{\cdot}4H_2O$.

2.2. The ionic concentrations of Mn-TCP and TCP extracts

To prepare the extracts of TCP and Mn-TCP: 2.0 g of Mn-TCP or TCP powders was fully dispersed in 10 mL of cell culture medium in a shaker at 37 °C with a speed of 120 rpm for 24 h. The solution was centrifuged at 4000 rpm for 10 min and the supernatant was taken. Then, the obtained extracts were filtered through a 0.22 μm filter to ensure sterility. Finally, we measured the concentrations of Ca, P and Mn with an inductively coupled plasma atomic emission spectroscopy (710 ES, Varian, USA). Pure culture medium without ionic extracts was used as control (CTR).

The gradient Mn^{2+} ion solutions were obtained by dissolving manganese chloride: 180 mg of $MnCl_2{\cdot}4H_2O$ was dissolved in 10 mL cell culture medium to obtain 100 mM Mn^{2+} ion solution. Then it was diluted to obtain different concentrations of Mn^{2+} ion solutions.

2.3. Antioxidant capability of Mn-TCP bioceramics

The superoxide anion, nitrogen free radicals and hydrogen peroxide scavenging activities were investigated to evaluate the antioxidant capability of Mn-TCP bioceramics. The superoxide anion scavenging activity was studied via a superoxide anion detection kit (A001-3, Nanjing Jiancheng Bioengineering Institute, China) following manufacturer's protocol. The absorbance of the final solution was measured by a UV–vis spectrophotometer at 550 nm. DPPH (1,1-diphenyl-2-picrylhydrazine) free radicals were used to study the nitrogen free radical scavenging activity of Mn-TCP bioceramics. In brief, 2 mg of DPPH was added into 48 mL of absolute ethyl alcohol to prepare DPPH working solution. And then Mn-TCP bioceramic were added into the DPPH working solution and stirred homogeneously. After 0.5 h of reacting at 37 °C, the absorbance of DPPH working solution was measured at 519 nm. Furthermore, hydrogen peroxide scavenging activity was investigated. Briefly, Mn-TCP bioceramic was added into 25 mM of hydrogen peroxide and reacted for 0.5 h. After centrifugation, the absorbance at 240 nm was measured with a Cary-60 UV–vis spectrophotometer.

2.4. Preparation of Mn-TCP and TCP bioceramic particle for in vivo study

The particles for *in vivo* study were prepared as the follow protocol. TCP/Mn-TCP bioceramic powders and polyvinyl alcohol solution were mixed homogeneously and compressed into Φ3 cm of discs. After 12 h of drying, the discs were sintered at 1100 °C for 3 h. Finally, the sintered discs were crashed and sieved to obtain the particles with a diameter of ~2 mm. Then, the TCP and Mn-TCP particles were sterilized via the high pressure steam sterilizer.

2.5. Cell viability assessment

In the whole study, RAW264.7 cells (American Type Culture Collection, Rockville, MD) and BMMs were cultured in DMEM medium and α-MEM (Gibco, Carlsbad, CA, USA) respectively, containing 10% FBS and 1% Penicillin-streptomycin solution. In addition, both cell types were induced with M-CSF (30 ng/mL) (R&D, Minneapolis, MN) and RANKL (50 ng/mL) (R&D, Minneapolis, MN) for osteoclastogenesis. BMMs were extracted from bone marrow of 4 weeks old C57BL/6 mice. For CCK8 assay (Dojindo Molecular Technologies, Tokyo, Japan), each well of 96-well plates was seeded with $3{\times}10^3$ cells and were treated with different dosages of Mn-TCP extracts, TCP extracts and Mn^{2+} ion

solutions for 24 h or 72 h. Then, we detected the cell viability at 450 nm. To detect cell apoptosis, BMMs were treated with Mn-TCP and TCP extracts at different dosages (0, 6.25 mg/mL, 50 mg/mL) for 3 d. The cells were resuspended in 100 μL PBS after washing in cold PBS for three times, and then stained with annexin V/7-ADD for 30 min in the dark. Fluorescent was detected by Flow Cytometry.

2.6. Osteoclastogenesis assays

In our study, mature OCs (nuclei number ≥3) normally started to form at 3 d and 7 d of RAW264.7 and BMMs, respectively. Therefore, osteoclastogenesis of RAW264.7 was measured at 24 h and 72 h and BMM osteoclastogenesis was detected at 3d and 7d.

OC differentiation was tested by Tartrate-Resistant Acid Phosphatase (TRAP) Staining. Each well of 96-well plate was seeded with 5×10^3 cells. BMMs and RAW264.7 were inducted for 7 d and 3 d respectively. The cells were stained with TRAP staining kit (Sigma, St. Louis, USA) according to the manufacturers' instructions.

Immunofluorescence staining of F-actin was used to reveal mature osteoclast formation. Each well of 96-well plate was seeded with 5×10^3 cells. BMMs were treated with the experimental dosages of Mn^{2+} ions for 7 d. Furthermore, BMMs were treated with the experimental dosages of the Mn-TCP and TCP extracts for 7 d respectively with the same method. Cells were stained with Actin Cytoskeleton and Focal Adhesion Staining Kit (Millipore, Darmstadt, Germany) according to the manufacturers' instructions. Nuclei were counterstained with DAPI (1:1000) for 5 min.

2.7. Pit formation assay

Uniformly inoculate 1×10^4 cells on each calf bone slice. BMMs were inducted with different concentration of Mn^{2+} ions for 9 d. Furthermore, BMMs were inducted with different concentration of Mn-TCP and TCP extracts for 9 d respectively with the same method. Then, the calf bone slices were washed with sodium hypochlorite bleach solution and stained with toluidine blue. The resorption area on bone slices was observed under the light microscope (Leica, DMIL LED).

2.8. ROS assay

Intracellular ROS levels were tested by ROS Assay Kit (Beyotime Biotechnology, Haimen, China). In short, dichloro-dihydro-fluorescein (DCFH) was oxidized to fluorescent DCF when ROS existed. Primary BMMs in 96-well plates were treated with different dosages of Mn^{2+}, Mn-TCP extracts and TCP extracts for 3 d respectively with a density of 5×10^3 cells per well. The cells were incubated with DCFH-DA (10 μM) for 20 min and then taken images by a fluorescence microscope (Bio-RAD, ZOE™ Fluorescent Cell Imager).

2.9. In vivo OVX-related femoral defect regeneration model

In this study, 3 month old female Sprague Dawley rats weighing 300–350 g were used. The use of all experimental animals and the experimental procedures involved in animal experiments had been approved by the Animal Center and Ethics Committee of Third Military Medical University (Chongqing, China, SYXK (PLA) 20170031). We tried our best to reduce the number of experimental animals and ease their suffering. All operations were carried out under sterile conditions. Penicillin (40000 IU/ml, 1 ml/kg) was injected daily for 3 consecutive days after operation to ensure no infection.

The osteoporotic rat model was established by bilateral ovariectomy. Eight weeks after the bilateral removal of the ovaries, a 2.5 mm defect in diameter was created at the lateral femoral condyle. TCP bioceramic particles and Mn-TCP bioceramic particles were implanted into the defects. These defects were randomized into three groups: blank group, TCP bioceramics group, Mn-TCP bioceramics group. The blank group was not implanted. Rats were sacrificed at 4 and 12 weeks after femoral surgery and femurs from each group were harvested for further examination, including Micro-CT analysis and histologic analysis.

2.10. Micro-CT and histologic analysis

Bruker MicroCT Skyscan 1176 system (Kontich, Belgium) was used for Micro-CT detection. Femurs that harvested at each time point were detected by Micro-CT. We can observe the establishment of the osteoporotic rat model and the specific microstructure changes. In addition, we can also observe new bone formation in the defect, and acquire 2D images and 3D reconstruction images.

For histologic analysis, femurs were decalcified in 10% EDTA (Sangon Biotech, Shanghai, China) by daily change for 8 weeks. The decalcified femurs were embedded in paraffin and cut into sections with a thickness of 4 μm, and then used for the hematoxylin and eosin (H&E) staining, Masson staining and TRAP immunohistochemical staining.

2.11. Detection of gene and protein expression

Gene expression was detected by RT-qPCR using PrimeScript Real-Time Reagent Kit (Takara, Kyoto, Japan) according to the manufacturer's instruction. Protein expression was detected by Western blot. Primary antibodies include rabbit antibodies against Keap1 (1:1000, Abcam, Cambridge, USA), nuclear factor-erythroid 2-related factor 2 (Nrf2) (1:1000, Bioword, China) and GAPDH (1:1000, Bioword) were used to detect proteins. The membrane was incubated with primary antibodies at 4 °C overnight and then further incubated with secondary antibody (1:1000, Cell Signaling Technology, Danvers, USA) for 1 h at room temperature. Immunofluorescence staining of Nrf2: Primary BMMs on circle microscope cover glass with diameter of 14 mm were treated with Mn^{2+} ions, Mn-TCP extracts or TCP extracts for 24 h, respectively. Subsequently, the cells were fixed with 4.0% paraformaldehyde and incubated with anti-Nrf2 rabbit polyclonal antibody (1:100, Bioss, Beijing, China) at 4 °C overnight, and then further incubated with Cy3-conjugated Affinipure Goat Anti-rabbit IgG antibody (1:100, Proteintech, Wuhan, China) for 1 h at room temperature. At last, the cells were treated with DAPI (Beyotime Biotechnology) for 5 min. The fluorescence images were obtained by Zeiss LSM 800.

2.12. Statistical analysis

Quantitative data are presented as means ± standard deviation (SD). One-way ANOVA followed with a Student-Newman-Keuls post hoc test was carried out to analysis the significant difference of multiple groups. Significant differences between the Mn-TCP extract groups and control groups were indicated as * $p < 0.05$ or ** $p < 0.01$. Significant differences between the TCP extract groups and control groups were indicated as $^{\#}p < 0.05$ or $^{\#\#}p < 0.01$. Significant differences between the Mn-TCP extract groups and TCP extract groups were indicated as $^{\blacktriangle}p < 0.05$ or $^{\blacktriangle\blacktriangle}p < 0.01$. Significant differences between the Mn^{2+} ions groups and control groups was indicated as * $p < 0.05$ or ** $p < 0.01$.

3. Results

3.1. Mn-TCP bioceramics significantly scavenged oxygen radicals and nitrogen radicals

Scanning electron microscope (SEM) and X-ray Diffraction (XRD) analyses were conducted for characterizing TCP and Mn-TCP. SEM images showed that there was no significant difference in grain morphology between TCP and Mn-TCP powders (Figs. S1A and B). Furthermore, XRD patterns displayed that TCP is beta phase of crystal form, and the incorporation of Mn did not change the crystal phase (Fig. S1C). The antioxidant properties of Mn-TCP bioceramics were investigated by conducting oxygen and nitrogen free radical scavenging experiments. To evaluate the superoxide anion scavenging effect of Mn-

TCP bioceramics, a superoxide anion detection kit was used. Digital photographs and UV–vis analysis indicated that compared to TCP bioceramics, Mn-TCP bioceramics could dramatically scavenge superoxide anions (Fig. 1A and B). A common radical, DPPH, was used to evaluate the nitrogen radical scavenging capability of Mn-TCP bioceramics. The results indicated that Mn-TCP bioceramics could significantly scavenge DPPH at the concentration of 50 mg mL^{-1} (Fig. 1C). Moreover, 25 mM hydrogen peroxide was further used to investigate the antioxidant capacity of Mn-TCP bioceramics. It was found that the characteristic absorbance of hydrogen peroxide at 240 nm significantly decreased after reacting with Mn-TCP bioceramics, while that of TCP bioceramics was not significantly different from that of 25 mM hydrogen peroxide (Fig. 1D).

3.2. The ion released from Mn-TCP and TCP bioceramics

The CTR group was pure culture medium, TCP and Mn-TCP extracts were obtained by soaking TCP and Mn-TCP powders in pure culture medium for 24 h, respectively. The concentrations of Mn, P and Ca in Mn-TCP and TCP extracts were measured by ICPAES, and the results are shown in Table S2. The concentration of Mn^{2+} ions in the Mn-TCP extract was 2.52 ppm, while there were barely any Mn^{2+} ions in the TCP extract and CTR group. The concentrations of Ca and P in CTR group were 15.67 and 38.71 ppm, respectively. The concentrations of Ca in the TCP and Mn-TCP extract were 17.18 ppm and 6.37 ppm. The concentrations of P in the Mn-TCP and TCP extracts were 8.06 ppm and 1.06 ppm, respectively. Since the ion release of bioceramics is a dynamic equilibrium process, the ion release and absorption simultaneously exist. Our results showed that the concentration of Ca in TCP extract was higher than pure culture medium, demonstrating that the Ca ions released from TCP powders were higher than those absorbed from pure culture medium. Furthermore, ion release and mineralization coexist during the TCP and Mn-TCP soaked in pure culture medium. During bioceramic mineralization, Ca and P play an important role. P in pure culture medium was participated in the mineralization process and absorbed to TCP and Mn-TCP powders, thus the concentrations of P in TCP and Mn-TCP extracts were both less than pure culture medium.

3.3. Mn-TCP extracts inhibited RANKL-induced osteoclastogenesis in vitro

Cell viability was measured by CCK8 assays. BMMs were induced with RANKL for 24 h or 72 h and treated with different doses of Mn-TCP and TCP extracts. RAW264.7 cells were treated in the same way. CCK8 assays indicated that Mn-TCP extracts decreased RAW264.7 cell viability at doses of 50 mg/mL or higher in the presence of RANKL (Fig. 2A and B). BMM viability was decreased when the dose of the Mn-TCP extracts reached 200 mg/mL (Fig. 2C and D).

In our study, OC differentiation was tested by TRAP staining (Fig. 2E, G). Mn-TCP extracts dose-dependently inhibited TRAP activity in both cell types. TCP extracts had no significant inhibitory effect on TRAP activity at concentrations lower than 100 mg/mL in BMMs and 50 mg/mL in RAW264.7 cells. Mn-TCP was better than TCP at inhibiting TRAP activity (Fig. 2F, H). We then selected two concentrations (6.25 mg/mL, 50 mg/mL) to evaluate the effects of Mn-TCP and TCP extracts on osteoclastogenesis in BMMs in subsequent experiments. The effects of Mn-TCP and TCP extracts on the cell apoptosis rate during BMM osteoclastogenesis were assessed by flow cytometry. Both TCP and Mn-TCP extracts inhibited cell apoptosis. However, there was no significant difference in the cell apoptotic rate between TCP and Mn-TCP extracts (Fig. 3A). Thus, we concluded that Mn^{2+} ions had no effect on the apoptosis of osteoclasts. Immunostaining of F-actin was used to reveal mature osteoclast formation. For BMM-induced osteoclastogenesis, the results showed that Mn-TCP extracts dose-dependently decreased the number of osteoclasts with actin rings, while the TCP extracts couldn't affect it (Fig. 3B and C). Furthermore, bone resorption was evaluated by pit formation assay. It showed that only Mn-TCP inhibited osteoclast resorptive function among the three groups (Fig. 3D). The results were further confirmed by quantification of the pit area proportions (Fig. 3E).

Consistent with previous results, the expression of the osteoclast-specific genes *NFATc1*, *c-Fos*, *MMP9*, *DC-STAMP*, *OC-STAMP*, *TRAP*, as well as *Ctsk* was downregulated in BMMs by Mn-TCP extracts under the induction of RANKL. And TCP extracts couldn't affect gene expression at either 3 d or 7 d (Fig. 4A–G). All of these results suggest that compared to the TCP bioceramic, the Mn-TCP bioceramic significantly inhibited osteoclast formation, resorptive function, and specific gene expression.

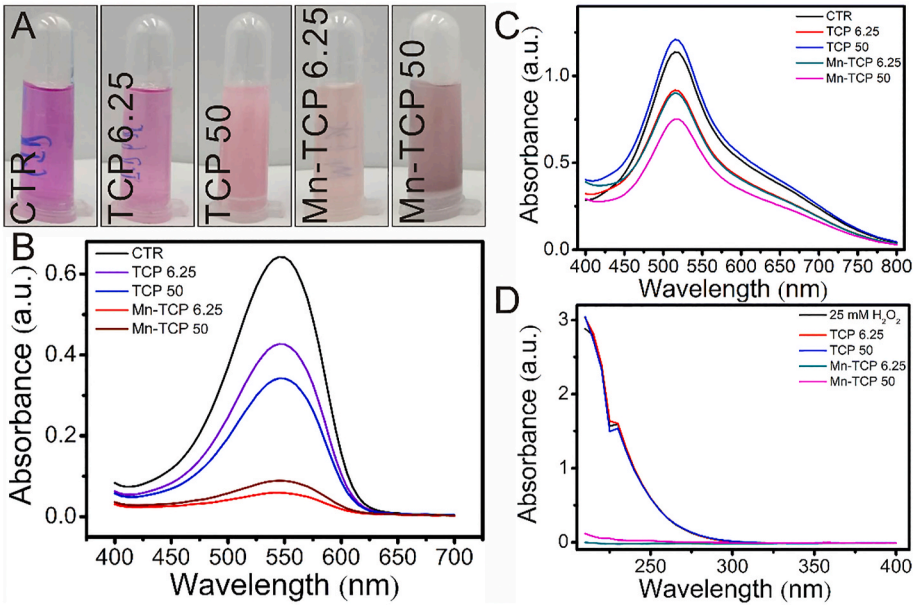

Fig. 1. Mn-TCP significantly scavenged multiple freeradicals. (**A**) photos of Mn-TCP scavenged superoxide radical, (**B**) superoxide radical scavenging, (**C**) DPPH scavenging, (**D**) H_2O_2 scavenging. Mn-TCP possessed the capability to scavenge superoxide radical, DPPH free radicals and H_2O_2. CTR: The group without any treatment was used as control. Mn-TCP 6.25/50: 6.25/50 mg Mn-TCP powders were added into per mL of working solution. TCP 6.25/50: 6.25/50 mg TCP powders were added into per mL of working solution.

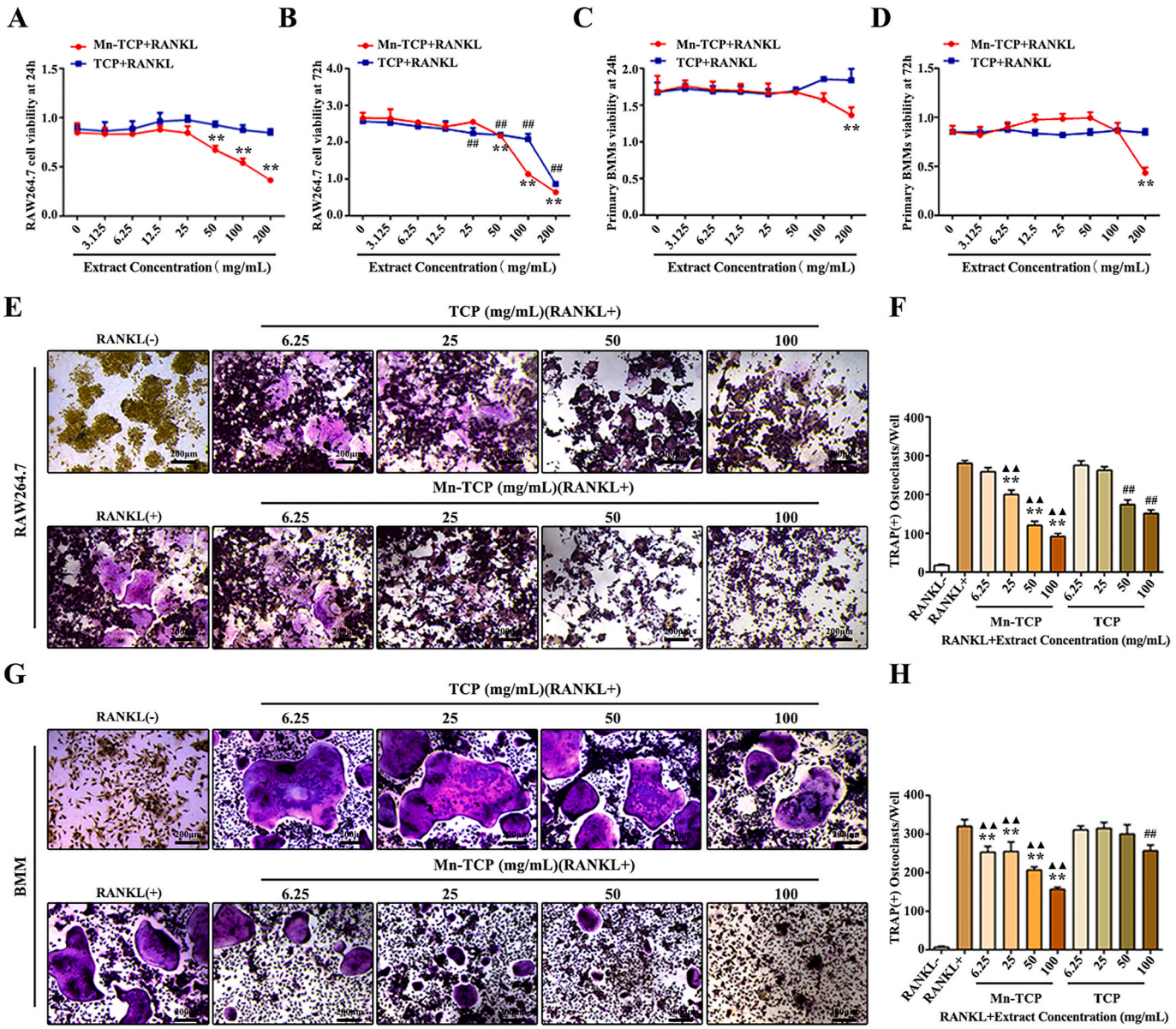

Fig. 2. Mn-TCP inhibits RANKL-induced osteoclast differentiation. (**A-D**) CCK-8 is used to detect RAW264.7 cells (**A**, **B**) and BMMs (**C**, **D**) cell viability, which are treated with different dosages of Mn-TCP and TCP extracts for 24 h and 72 h, (**E**) TRAP stain during osteoclastogenesis of RAW264.7 cells, which are treated with Mn-TCP and TCP extracts for 72h, (**F**) Quantification of TRAP(+) cells in each well, (**G**) TRAP stain during osteoclastogenesis of BMMs, which are treated with Mn-TCP and TCP extracts for 7 d, (**H**) Quantification of TRAP(+) cells in each well.

3.4. Mn^{2+} ions inhibited RANKL-induced osteoclastogenesis in vitro

Mn^{2+} ions with various concentrations were used in cell culture for 3 d and 7 d to study the effect of Mn^{2+} ion on osteoclast formation of BMMs. The CCK8 assay results indicated that Mn^{2+} ions started to decrease cell viability at doses of 25 μM or higher at 3 d and 7 d (Figs. S2A and B). Therefore, we selected 1 μM and 10 μM in subsequent experiments. The flow cytometry results showed that the concentration of Mn^{2+} ions (1 μM and 10 μM) had no effect on the apoptotic rate of osteoclasts at either 3 d or 7 d (Fig. S2C). The TRAP staining, F-actin immunostaining and pit formation assay results demonstrated that Mn^{2+} ions inhibited osteoclast formation, osteoclast fusion and osteoclastic bone resorption (Fig. 5A–C). Quantitative analysis indicated that Mn^{2+} ions inhibited RANKL-induced osteoclast formation (Fig. 5D–F). Furthermore, several osteoclast-specific gene expressions were significantly decreased during osteoclastogenesis following the addition of Mn^{2+} ions (Figs. S3A–G).

Mn-TCP bioceramics inhibited RANKL-induced osteoclastogenesis through activating Nrf2 and scavenging ROS.

According to our previous study, the Mn-TCP bioceramic could scavenge both superoxide anion and hydrogen peroxide *in vitro*. Several studies have shown that ROS are an important contributor to the formation and differentiation of osteoclasts. As a key redox-sensitive transcription factor, Nrf2 is reported to inhibit RANKL-induced osteoclastogenesis by downregulating intracellular ROS levels [32]. As an endogenous inhibitor of Nrf2, Keap1 (Kelch-like ECH-associated protein 1) binds to Nrf2 in the cytoplasm, leading to its ubiquitination and degradation [33]. Therefore, to uncover the mechanism of Mn-TCP bioceramics inhibited osteoclastogenesis, intracellular ROS production in BMMs was measured after treatment with Mn-TCP and TCP extracts and Mn^{2+} ions. The results indicated that 6.25 mg/mL and 50 mg/mL Mn-TCP extracts markedly decreased ROS levels. The ROS level was slightly decreased by TCP extracts only at the concentration of 50 mg/mL (Fig. 6A). In addition, the scavenging effects of Mn^{2+} ions on

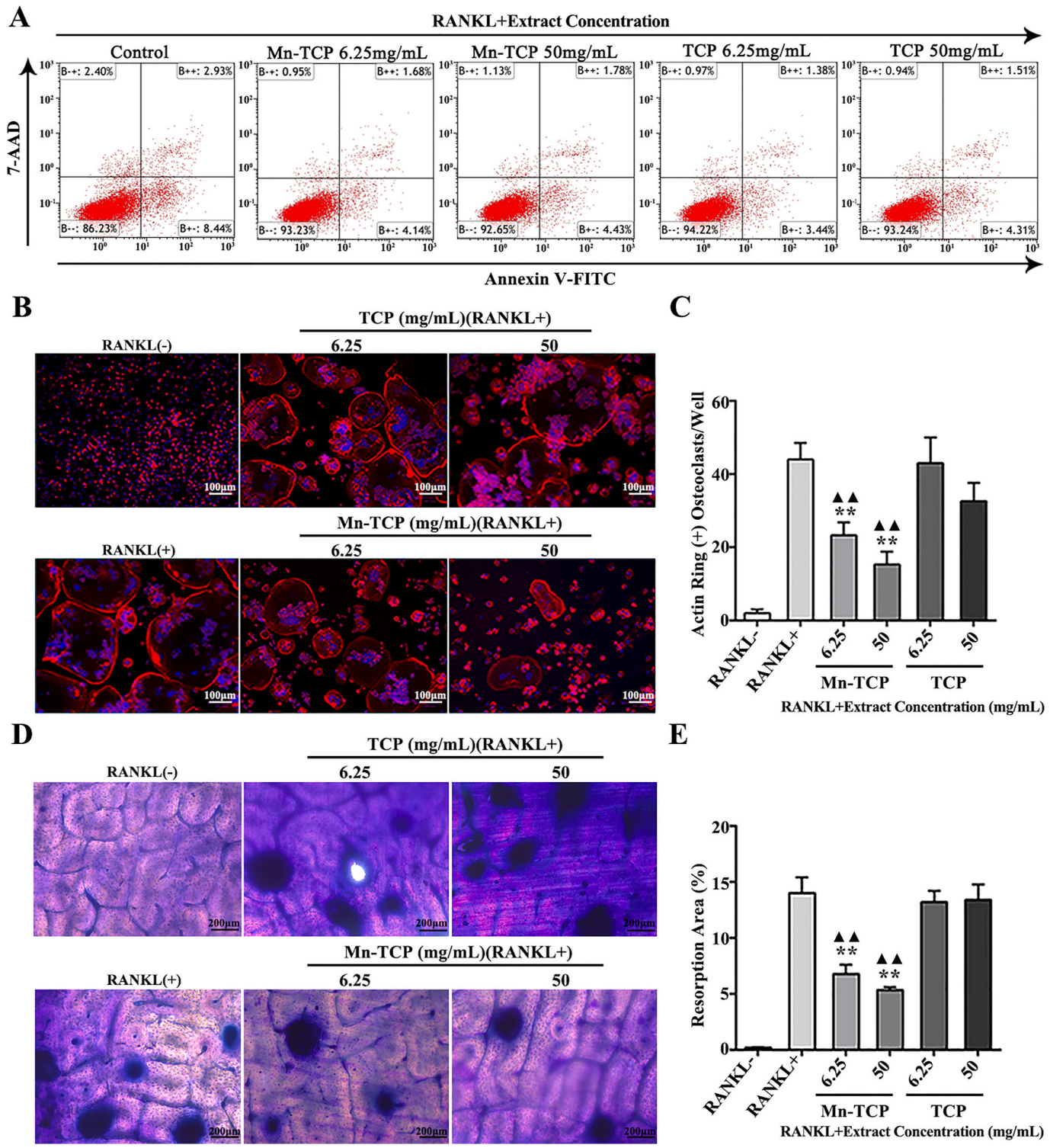

Fig. 3. Mn-TCP inhibits osteoclast function during osteoclastogenesis of BMMs which are induced by RANKL. (**A**) FCM shows the cell apoptosis rate during osteoclastogenesis of BMMs, which are treated with different dosages of (6.25 mg/mL, 50 mg/mL) of Mn-TCP and TCP extracts for 3d. (**B**) F-actin immunofluorescence staining during osteoclastogenesis of BMMs, which are stimulated with different dosage (6.25 mg/mL, 50 mg/mL) of Mn-TCP and TCP extracts for 7 d, (**C**) Quantitative analysis of actin ring (+) osteoclasts in each well, (**D**) Pit formation assay during osteoclastogenesis of BMMs at 9 d, (**E**) Quantitative analysis of resorption area proportion.

ROS production were examined. The results showed that Mn^{2+} ions inhibited ROS production in a dose-dependent manner (Fig. 6B). Additionally, qRT-PCR was used to measure Nrf2 expression at 3 d and 7 d of RANKL-induced osteoclastogenesis. Both Mn-TCP extracts and Mn^{2+} ions upregulated the expression of Nrf2 (Fig. 6C and D). Furthermore, immunofluorescence staining indicated that the nuclear translocation of Nrf2 could be promoted by the treatment of Mn-TCP extracts and Mn^{2+} ions (Figs. S4A and B). Western blot analysis demonstrated that Mn-TCP extracts significantly enhanced the protein level of Nrf2, and slightly downregulated the level of Keap1. There was no significant difference in

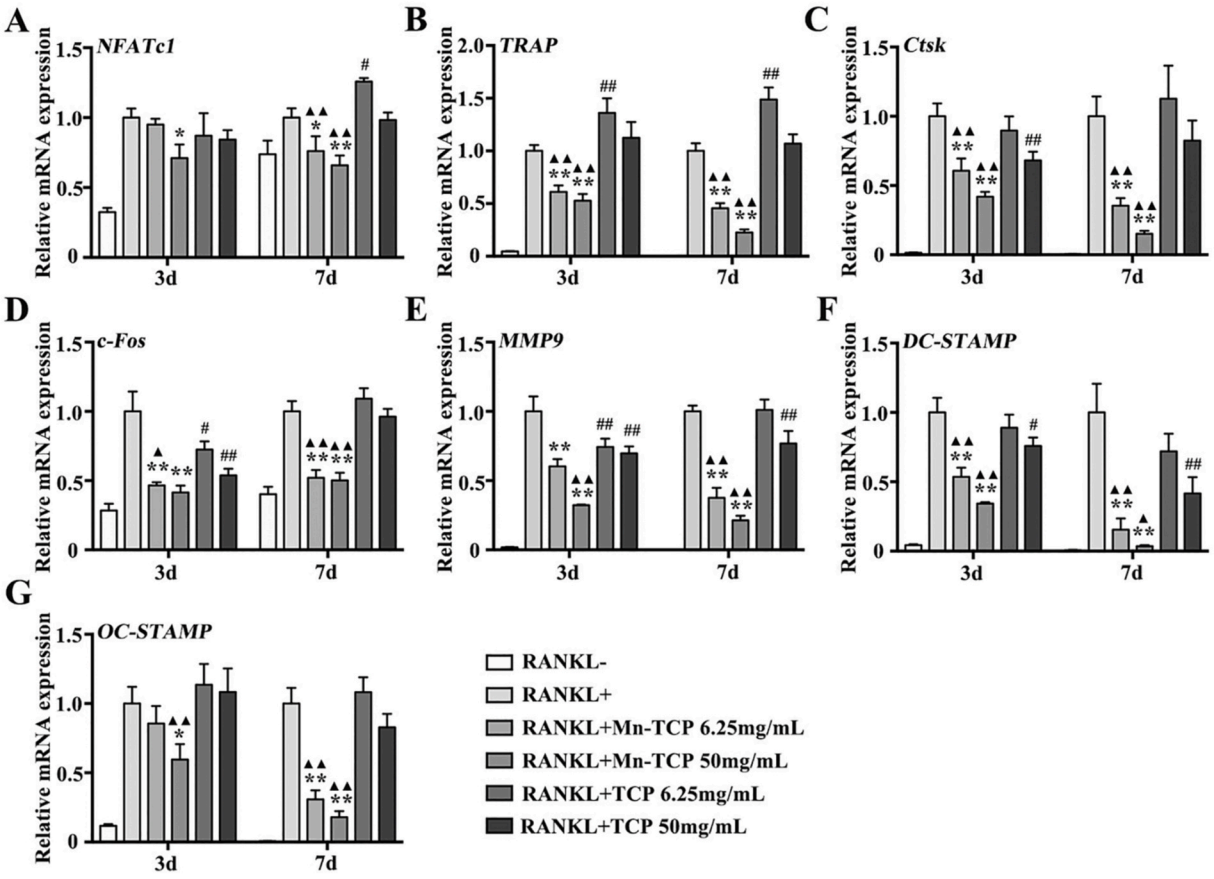

Fig. 4. The relative genes expression of *NFATc1*, *c-Fos*, *MMP9*, *DC-STAMP*, *OC-STAMP*, *TRAP*, and *Ctsk* during osteoclatogenesis of BMMs under the treatment of different dosages (6.25 mg/mL, 50 mg/mL) of Mn-TCP and TCP extracts for 3 d and 7 d.

the protein level of Nrf2 and Keap1 under the treatment of TCP extracts (Fig. 6E). In addition, to further prove that Mn-TCP extracts could activate the Nrf2 signaling pathway, brusatol as the specific inhibitor of Nrf2 was used as a control in this study. CCK8 analysis indicated that brusatol decreased BMMs cell viability at doses of 40 nM and higher (Fig. S4 C). 20 nM of brusatol was used for the experiment. The Western blot results suggested that Mn-TCP extracts increased the expression of Nrf2 and its downstream antioxidant enzymes, such as catalase and SOD2. However, after specific inhibition of Nrf2, the expression of catalase and SOD2 induced by Mn-TCP extracts decreased significantly (Fig S4 D). It indicated that Mn-TCP extracts could activate the Nrf2 signaling pathway.

3.5. Mn-TCP bioceramics stimulated the bone regeneration of OVX rats

We determined the *in vivo* inhibition of bone resorption and the regeneration of osteoporotic bone defects by Mn-TCP bioceramics. First, we examined the effect of Mn-TCP bioceramics on the osteogenic differentiation of MC3T3-E1 cells *in vitro*. The results showed that both Mn-TCP bioceramics and TCP bioceramics promoted the expression of ALP and calcium nodules, which was higher in the Mn-TCP bioceramic group than in the TCP bioceramic group (Figs. S5A and B). The upregulation of ALP activity and the increase in mineralized nodule indicated the maturation of osteoblasts. Then, we established an osteoporotic model of OVX rats *in vivo*. The Mn-TCP and TCP bioceramic particles with a diameter of ~2 mm were used for *in vivo* regeneration (Fig. S6A). The SEM analysis was conducted to observe the morphology of the bioceramic particles. It showed that the Mn-TCP and TCP bioceramic particles possessed rough surfaces (Fig. S6B). The operation time points are shown in Fig. 7A. 2D projection images revealed that the volume and density of trabecular bone were significantly decreased, the separation of trabecular bone was markedly increased, the trabecular microstructure was disordered, and the bone marrow cavity was enlarged in OVX rats compared to those of sham-operated rats (Fig. 7B). H&E staining and Masson staining also indicated obvious changes between Sham rats and OVX rats. For example, the bone trabeculae of Sham rats presented plate-like structure and the bone trabeculae of OVX rats presented rod-like structure (Fig. 7C).

Representative images of new bone formation in the femur defects in each group were obtained by 3D reconstruction. The 3D images clearly depicted the differences among the three groups. Four weeks after femur defect induction, new bone formation was observed in the defects of all the groups (Fig. 7D_1-F_4). Compared with the unfilled defects, the bioceramics groups showed significantly improved new bone quantity (Fig. 7D_2, E_4 and F_4). In addition, the results of histological analysis were consistent with that of micro-CT analysis. New bone formation was observed by H&E staining and Masson staining. In the Control group (without any implantation), there was nothing but some sparsely distributed fibrous tissue within defect sites (Fig. 7G, J). In the bioceramics group, bone regeneration was observed at the defect sites that were filled with bioceramics, and there were more new bone tissues in Mn-TCP bioceramics group (Fig. 7I, L) than in the TCP bioceramics group (Fig. 7H, K). Furthermore, compared with the Control group, both TCP and Mn-TCP bioceramic groups showed significantly improved bone volume fraction (BV/TV) and trabecula number (Tb.N) (Figs. S7A and B), and the marked decrease in trabecular separation (Tb.Sp) (Fig. S7C). However, There was no significant difference between Mn-TCP and TCP bioceramics in the Micro-CT parameters of bone regeneration within femur defects at 4 weeks of postimplantation (Figs. S7A–C). Moreover, TRAP immunohistochemical staining was used

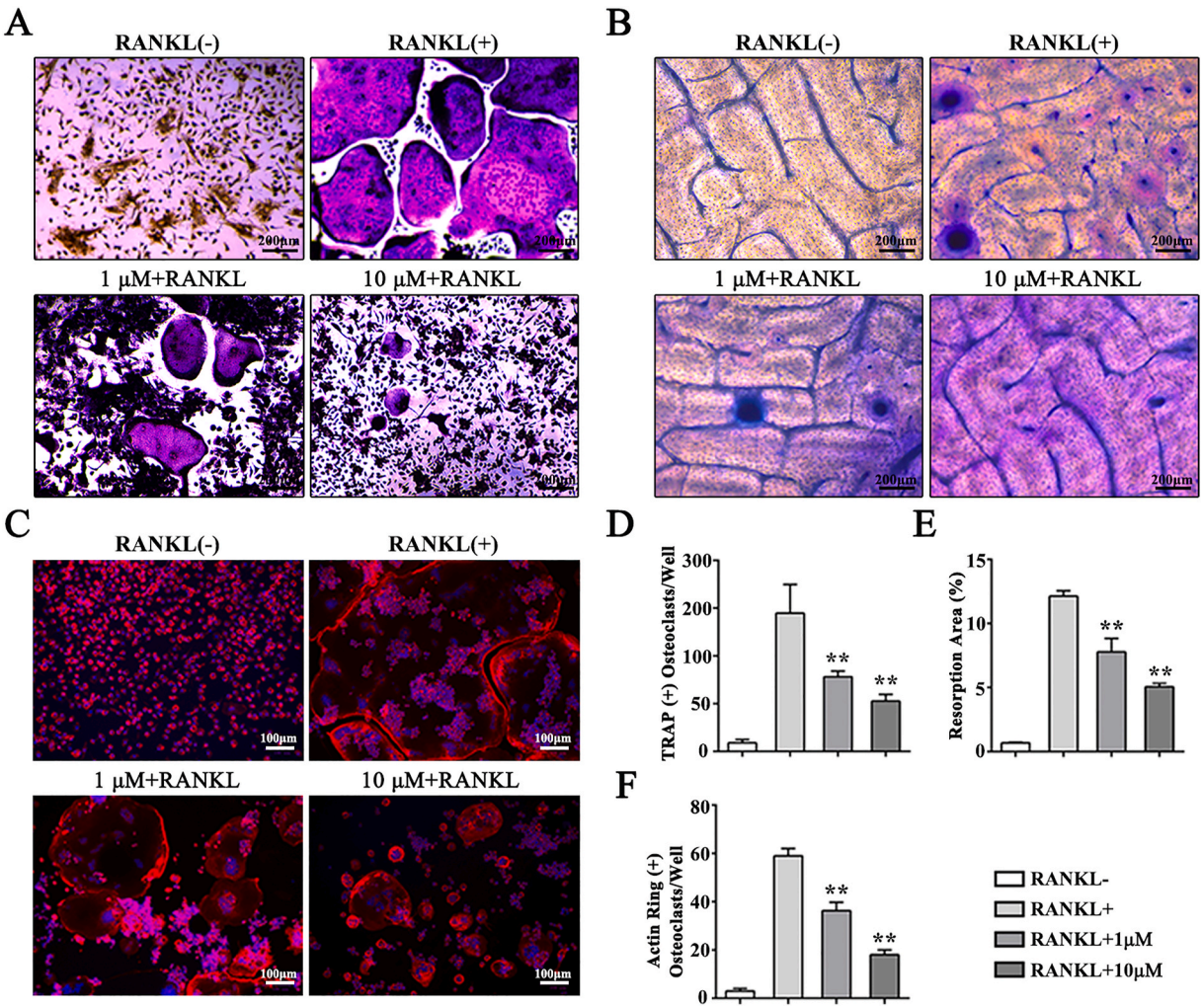

Fig. 5. Mn^{2+} ions inhibit RANKL-induced osteoclastogenesis of BMMs. (A) TRAP stain applied to detect osteoclasts differentiation of BMMs treated with different dosage of Mn^{2+} ions (1 μM, 10 μM) for 7 d, (**B**) Pit formation assay is used to evaluate osteoclast function at 9 d, (**C**) F-actin immunofluorescence staining during osteoclastogenesis of BMMs, which are treated with different dosage of Mn^{2+} ions (1 μM, 10 μM) for 7 d, (**D**) Quantitative analysis of TRAP (+) cells in each well, (**E**) Quantitative analysis of actin ring (+) osteoclasts in each well, (**F**) Quantitative analysis of resorption area proportion on bone slices.

to observe osteoclasts conditions. Osteoclasts were observed surrounding and within the defect area. The number of osteoclasts was the lowest in Mn-TCP bioceramics group (Fig. 7M–O).

At 12 weeks after femur defect induction, both 3D and histological images showed similar bone regeneration results as those at 4 weeks after defect induction (Fig. 8A–I). However, bone regeneration in the 12-week groups was better than that in the 4-week groups. The 3D images demonstrated that the Control group exhibited poor regeneration (Fig. 8A_1, A_2). The Mn-TCP bioceramics group (Fig. 8C_1, C_4) exhibited more newly regenerated bone than the TCP bioceramics group (Fig. 8B_1, B_4). H&E and Masson staining indicated little new bone tissue in the defects of Control group (Fig. 8D, G). A certain amount of new bone tissue was observed around the defect area in the TCP bioceramic group. However, large vacant spaces were still present in the center of the defect region (Fig. 8E, H). The new bone tissue in the Mn-TCP bioceramic group was evenly distributed throughout the defect site, including the center of the defect region (Fig. 8F, I). Furthermore, at 12 weeks, compared with the TCP bioceramic group and Control group, Mn-TCP bioceramic group showed significantly increased in bone mineral density (BMD), the relative bone volume fraction (BV/TV) and trabecula number (Tb.N) (Fig. 8J-L). In addition, a marked decrease in trabecular separation (Tb.Sp) was observed in the Mn-TCP bioceramic group compared to the Control group and TCP bioceramic group (Fig 8M).

4. Discussion

Bones are dynamic living tissues that constantly renew throughout life. The dynamic balance of bone depends on remodelling mediated by osteoblasts and osteoclasts [34]. An imbalance between osteoblastic bone production and osteoclastic bone resorption leads to multiple bone diseases. The pathogenesis of these diseases, such as Paget's disease, cancer bone metastasis, multiple myeloma, and especially osteoporosis, is thought to be caused by the activation of osteoclasts [35]. In this context, inhibiting osteoclast differentiation may be a powerful tool for treating these diseases. Studies have shown that bisphosphonates, oestrogen and calcitonin are the main pharmacological methods for the treatment of osteoporosis by inhibiting osteoclast activity. However, long-term use of these drugs might cause constipation, diarrhoea, tumorigenesis and cardiovascular effects, as well as osteonecrosis of the jaw [36,37]. Therefore, finding new strategies to inhibit osteoclast differentiation and osteoclastic activity for treating osteoporosis and related diseases is urgently needed. In this study, we elucidated for the first time that the bioceramic Mn-TCP inhibited osteoclastogenesis and promoted osteoporotic bone defect regeneration by activating Nrf2 and suppressing ROS.

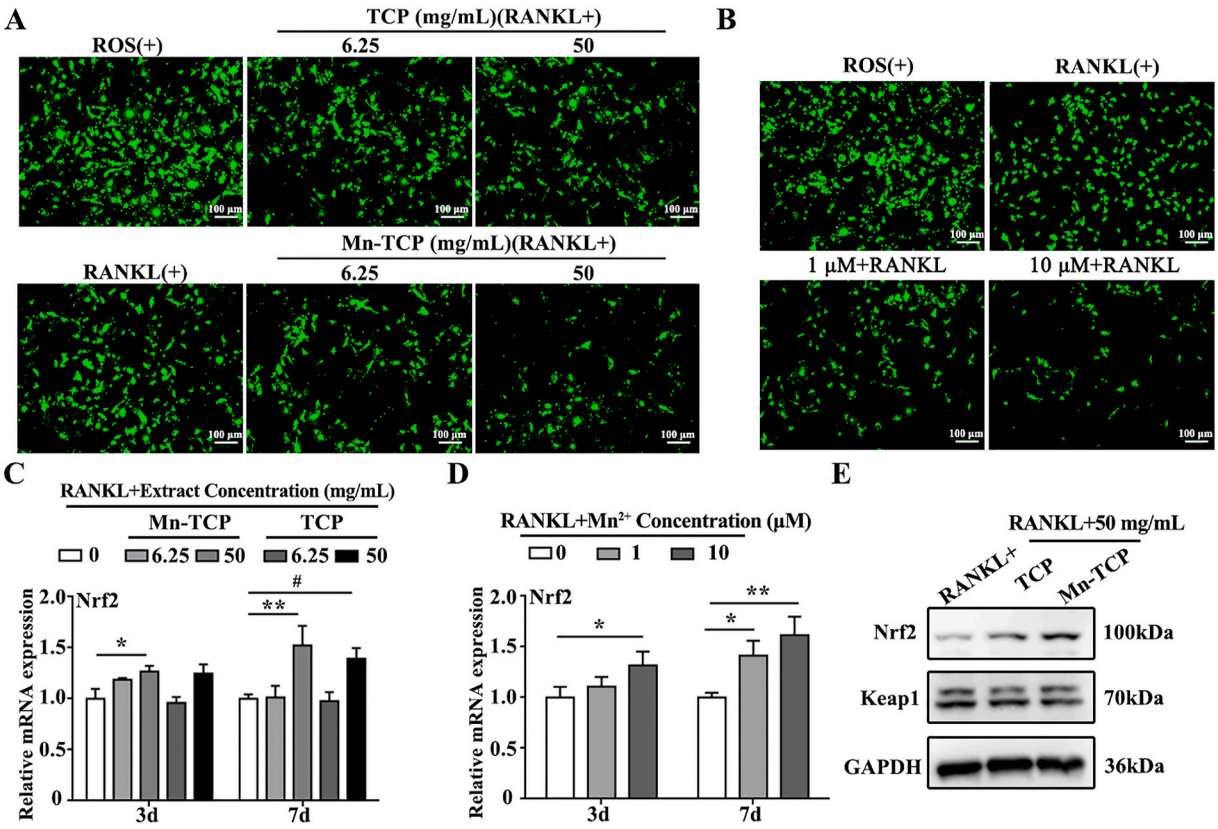

Fig. 6. Mn-TCP extracts and Mn^{2+} ions scavenge ROS generation and activate Nrf2 expression during RANKL-induced osteoclastogenesis of BMMs. (**A**) Fluorescence images of ROS positive during osteoclastogenesis of BMMs, which are treated with different concentrations (6.25 mg/mL, 50 mg/mL) of Mn-TCP and TCP extracts for 3 d, (**B**) Fluorescence images of ROS positive during osteoclastogenesis of BMMs, which are treated with different concentrations of Mn^{2+} ions (1 μM, 10 μM) for 3 d, (**C**) Relative mRNA expression levels of Nrf2 during osteoclastogenesis of BMMs under the treatment of different concentrations (6.25 mg/mL, 50 mg/mL) of Mn-TCP and TCP extracts for 3 d and 7 d, (D) Relative mRNA expression levels of Nrf2 during osteoclastogenesis of BMMs under the treatment of different concentrations of Mn^{2+} ions (1 μM, 10 μM) for 3 d and 7 d, (E) The protein level of Nrf2 and Keap1 during osteoclastogenesis of BMMs under the treatment of Mn-TCP and TCP extracts for 5 d.

In this study, Mn-TCP bioceramics were successfully prepared using TCP as a substrate and applied to regenerate bone defects in rats with osteoporosis. TCP has been widely used in bone regeneration due to its osteoconductive and osteoinductive characteristics. Both of the activation of osteoblasts and osteoclasts were regulated by the released calcium and phosphorus [38]. In addition, Mn^{2+} ions have attracted attention in bone regeneration due to their ability to promote osteogenic differentiation and maintain bone mass [27,28]. Moreover, a previous study showed that rats fed a long-term manganese-depleted diet exhibited significantly decreased ectopic osteogenesis [39]. Ries and colleagues exhibited that bone resorption could be suppressed by an isolated osteoclast system which was called as Desferal-manganese complex, whereas, the system could not function without Mn [40]. In this study, we constructed a Mn-containing scaffold using TCP as a substrate, which could stably release Mn^{2+} ions to meet the long-term ionic demand of osteoporotic bone regeneration. The results suggested that the Mn-TCP bioceramic could inhibit osteoclastogenesis and bone resorptive functions by down-regulate the expression of osteoclast-specific genes and markers. Moreover, compared with the pure TCP group, Mn-TCP bioceramic could upregulate ALP expression and accelerate the formation of calcium nodules in MC3T3-E1 cells, during osteogenic differentiation. It demonstrated that Mn-TCP promoted osteogenic differentiation of MC3T3-E1 cells. Furthermore, the *in vivo* study showed that the Mn-TCP bioceramic promoted bone defect regeneration in rats suffering from osteoporosis compared to those in the pure TCP group. These results suggest that Mn is a potential treatment for osteoporosis, and the combination of calcium phosphate and Mn has great potential for the regeneration of osteoporotic bone defects.

Oxidative stress, as a factor that affects bone remodelling, accelerates osteoporosis progression and plays a crucial role in the functional and morphological changes in osteoclasts in osteoporosis [41,42]. ROS, particularly hydrogen peroxide, are important contributors to the formation and differentiation of osteoclasts [43]. Moreover, increased ROS in bone marrow-derived monocytes or macrophages could accelerate the formation of osteoclasts by activating TNFα, TRAF6 and Rac1 [44]. Scavenging ROS inhibited RANKL-induced osteoclastogenesis and suppressed ovariectomy-induced osteoporosis [11,13,14]. In addition, high levels of ROS could deter osteogenesis differentiation of BMSCs and inhibit normal bone regeneration. Hence, it is of great importance to scavenge ROS to efficiently regenerate bone defects in osteoporosis [45]. In our study, Mn-TCP bioceramics were found to effectively scavenge superoxide anions, hydrogen peroxide and DPPH free radicals, inhibit osteoclast activity and promote osteogenic differentiation. With both superoxide anion and hydrogen peroxide scavenging properties, the Mn-TCP bioceramic could transform superoxide anion directly into oxygen and water, avoiding the accumulation of hydrogen peroxide, which prevents osteoclast differentiation and benefits osteogenic differentiation. Therefore, the Mn-TCP bioceramic could scavenge ROS by transforming ROS into oxygen and water, which might be beneficial for osteoporotic bone defect regeneration.

Keap1-Nrf2 pathway is the main antioxidant defense mechanism trigged by Nrf2 [46]. The activation of Nrf2 leads to a decrease in intracellular ROS levels by regulating different antioxidant enzymes [47,48]. In addition, it has been reported that an appropriate amount of Mn^{2+} ions can significantly increase the levels of superoxide dismutase and peroxidase in tomato seedlings [31]. Therefore, we hypothesized

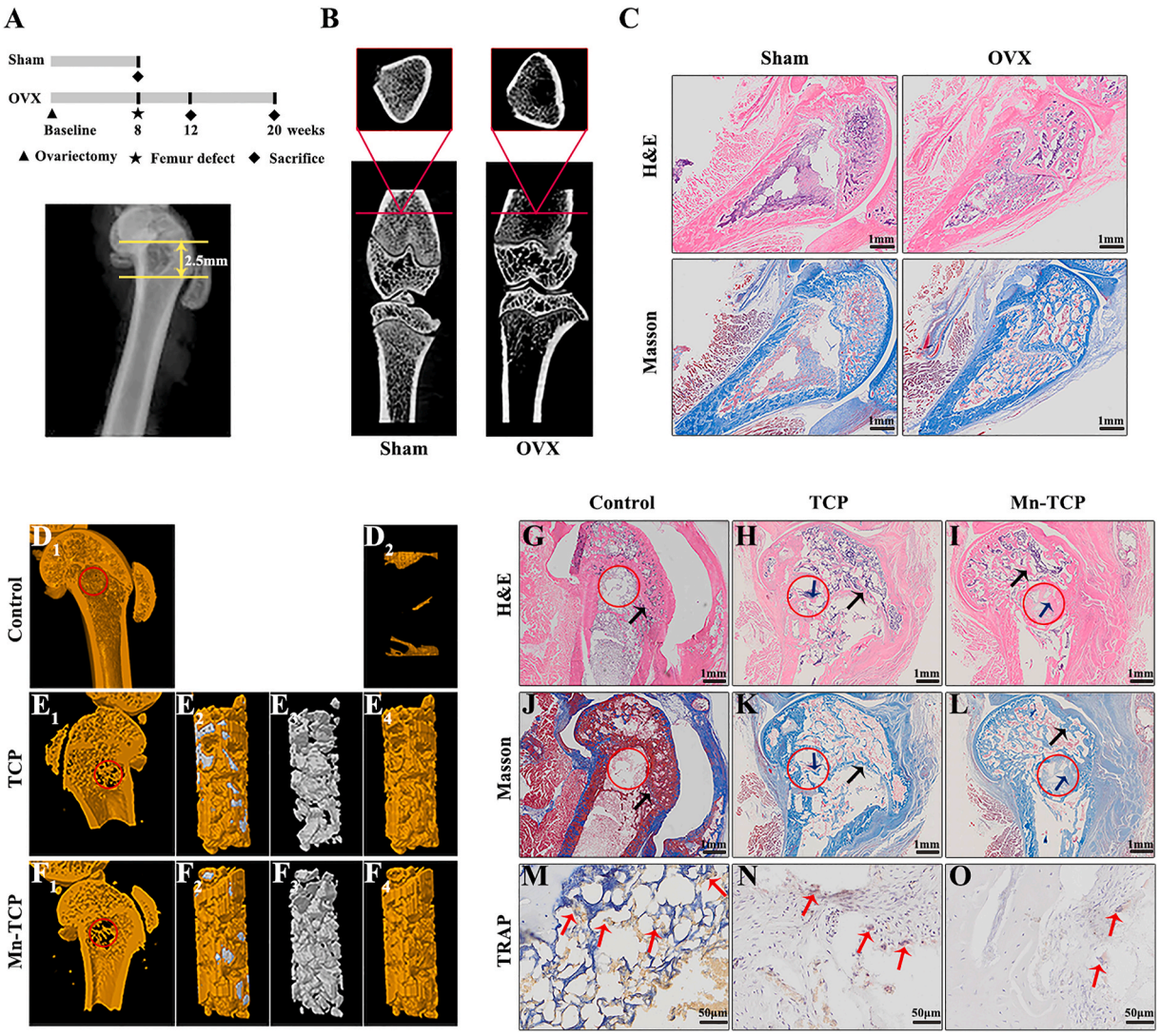

Fig. 7. Mn-TCP bioceramics promote osteoporotic bone defect regeneration in OVX rats at 4 weeks postimplantation. (A) Schematic diagram of the surgery time points, (B) 2D images showed the normal and osteoporotic bone, (C) H&E staining and Masson staining in Sham group and OVX group, (D_1-F_4) 3D reconstruction images of Control group, Mn-TCP bioceramics group and TCP bioceramics group. D_1 and D_2: Control group without implantation, E_1-E_4: TCP bioceramics group, F_1–F_4: Mn-TCP bioceramics group. E_2 and F_2: 3D reconstruction images of bioceramics and new bone, E_3 and F_3: 3D reconstruction images of bioceramics, D_2, E_4 and F_4: 3D reconstruction images of new bone, (G–I) H&E staining for all the groups, (J–L) Masson staining for all the groups, (M–O) TRAP staining for all the groups. The red circle represents the defect area. The red arrow represents osteoclasts. The black arrow represents the host bone. The blue arrow represents the new bone (n = 3).

that Mn-TCP bioceramic could scavenge ROS by activating Nrf2 to regulate antioxidant enzymes. In this study, Mn-TCP bioceramics were found to upregulate the expression of Nrf2 and promote its nuclear translocation. Meanwhile, the endogenous inhibitor of Nrf2, Keap1 slightly decreased with Mn-TCP bioceramics. In addition, the antioxidant enzymes catalase and SOD2 were also increased by Mn-TCP extracts. However, after specific inhibition of Nrf2 by brusatol, the expression of catalase and SOD2 induced by Mn-TCP extracts decreased significantly. The results indicated that Mn-TCP bioceramics could activate Nrf2 and lead to its target gene expression, so as to scavenge ROS. Our results did show that Mn-TCP bioceramics significantly decreased intracellular ROS levels. Thus, Mn-TCP bioceramic-induced bone regeneration in osteoporotic rats was thought to be related to Mn^{2+}-mediated promotion of osteogenic differentiation and inhibition of osteoclast formation and resorptive function by scavenging ROS through Nrf2 activation.

5. Conclusion

In summary, Mn-containing bioceramics were prepared by combining Mn with TCP bioceramics and used to regenerate bone defects in rats suffering from osteoporosis. The introduction of Mn^{2+} ions not only endows TCP bioceramics with the ability to scavenge ROS but also inhibits the formation and function of osteoclasts *in vitro*. Moreover, Mn^{2+} ions released from Mn-TCP bioceramics can significantly enhance ALP activity and the mineralization of MC3T3-E1 cells. Additionally, Mn-TCP bioceramics decreased the number of osteoclasts and accelerated bone defect regeneration in osteoporotic rats by activating Nrf2 and scavenging ROS. Our study suggests that Mn-containing bioceramics can be further applied as a biomaterial to promote bone regeneration for treating osteoporotic bone defects.

CRediT authorship contribution statement

Jianmei Li: Conceptualization, Validation, Writing – review & editing, Funding acquisition. **Cuijun Deng:** Writing – review & editing,

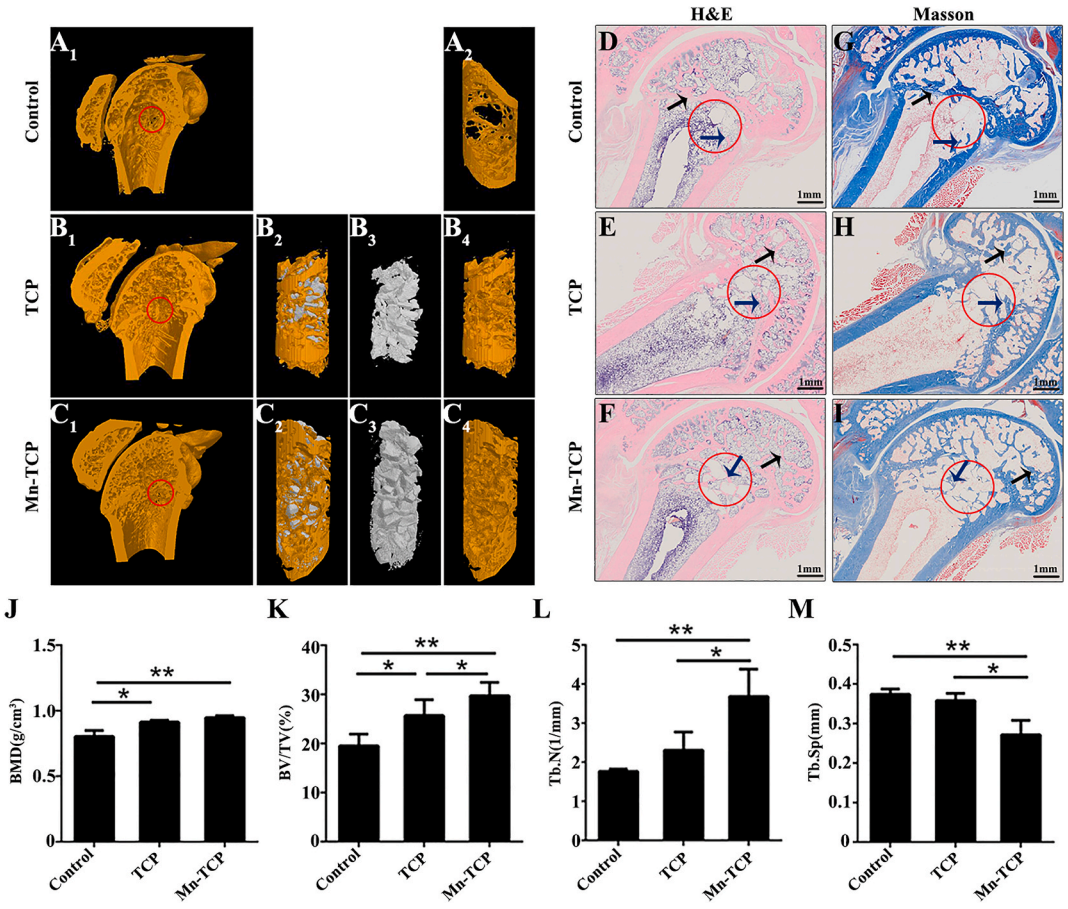

Fig. 8. Mn-TCP bioceramics promote osteoporotic bone defect regeneration in OVX rats at 12 weeks postimplantation. (A_1-C_4) 3D reconstruction images of Control group, Mn-TCP bioceramics group and TCP bioceramics group. A_1 and A_2: Control group without implantation, B_1–B_4: TCP bioceramics group, C_1–C_4: Mn-TCP bioceramics group. B_2 and C_2: 3D reconstruction images of bioceramics and new bone, B_3 and C_3: 3D reconstruction images of bioceramics, A_2, B_4 and C_4: 3D reconstruction images of new bone, (**D-F**) H&E staining for all the groups, (**G-I**) Masson staining for all the groups, (**J-M**) Micro-CT parameters of bone regeneration within femur defects. The red circle represents the defect area. The black arrow represents the host bone. The blue arrow represents the new bone (n = 3).

Validation. **Wanyuan Liang:** Data curation. **Fei Kang:** Methodology, Funding acquisition. **Yun Bai:** Methodology. **Bing Ma:** Data curation. **Chengtie Wu:** Writing – review & editing, Supervision. **Shiwu Dong:** Conceptualization, Writing – review & editing, Supervision, Funding acquisition.

Declaration of competing interest

No conflict of interest exits in the submission of this manuscript, and manuscript is approved by all authors for publication. I would like to declare on behalf of my co-authors that the work described was original research that has not been published previously, and not under consideration for publication elsewhere, in whole or in part. All the authors listed have approved the manuscript that is enclosed. I hope this paper is suitable for "***Bioactive Materials***".

Acknowledgements

This work was funded by project supported by the Key Program of National Natural Science Foundation of China (81930067), the Youth Program of National Natural Science Foundation of China (grant number 82002316), the Youth Cultivation Project of Army Medical University (2020XQN08) and General Program of Natural Science Foundation of Chongqing (cstc2019jcyj-msxmX0176).

Appendix A. Supplementary data

Supplementary data to this article can be found online at https://doi.org/10.1016/j.bioactmat.2021.03.039.

References

[1] D.M. Black, E.J. Geiger, R. Eastell, et al., Atypical femur fracture risk versus fragility fracture prevention with bisphosphonates, N. Engl. J. Med. 383 (8) (2020) 743–753.
[2] C. Binding, J. Bjerring Olesen, B. Abrahamsen, et al., Osteoporotic fractures in patients with atrial fibrillation treated with conventional versus direct anticoagulants, J. Am. Coll. Cardiol. 74 (17) (2019) 2150–2158.
[3] R. Bartl, C. Bartl, Bone Disorders (2017), https://doi.org/10.1007/978-3-319-29182-6.
[4] X. Chen, X. Zhi, P. Pan, et al., Matrine prevents bone loss in ovariectomized mice by inhibiting RANKL-induced osteoclastogenesis, Faseb. J. 31 (11) (2017) 4855–4865.
[5] C. Dou, N. Ding, C. Zhao, et al., Estrogen deficiency-mediated M2 macrophage osteoclastogenesis contributes to M1/M2 ratio alteration in ovariectomized osteoporotic mice, J. Bone Miner. Res. 33 (5) (2018) 899–908.
[6] Y. Gao, W. Ge, The histone methyltransferase DOT1L inhibits osteoclastogenesis and protects against osteoporosis, Cell Death Dis. 9 (2) (2018) 33.
[7] S.L. Teitelbaum, Stem cells and osteoporosis therapy, Cell Stem Cell 7 (5) (2010) 553–554.
[8] J. Li, Q. Wang, R. Yang, et al., BMI-1 mediates estrogen-deficiency-induced bone loss by inhibiting reactive oxygen species accumulation and T cell activation, J. Bone Miner. Res. 32 (5) (2017) 962–973.
[9] K. Chen, P. Qiu, Y. Yuan, et al., Pseurotin A inhibits osteoclastogenesis and prevents ovariectomized-induced bone loss by suppressing reactive oxygen species, Theranostics 9 (6) (2019) 1634–1650.
[10] S. Maria, R.M. Samsonraj, F. Munmun, et al., Biological effects of melatonin on osteoblast/osteoclast cocultures, bone, and quality of life: implications of a role for

MT2 melatonin receptors, MEK1/2, and MEK5 in melatonin-mediated osteoblastogenesis, J. Pineal Res. 64 (3) (2018).
[11] Y. Liu, C. Wang, G. Wang, et al., Loureirin B suppresses RANKL-induced osteoclastogenesis and ovariectomized osteoporosis via attenuating NFATc1 and ROS activities, Theranostics 9 (16) (2019) 4648–4662.
[12] H.S. Kim, S.T. Nam, S.H. Mun, et al., DJ-1 controls bone homeostasis through the regulation of osteoclast differentiation, Nat. Commun. 8 (1) (2017) 1519.
[13] C. Dou, Z. Cao, N. Ding, et al., Cordycepin prevents bone loss through inhibiting osteoclastogenesis by scavenging ROS generation, Nutrients 8 (4) (2016) 231.
[14] Q. Ma, M. Liang, X. Tang, F. Luo, C. Dou, Vitamin B5 inhibit RANKL induced osteoclastogenesis and ovariectomy induced osteoporosis by scavenging ROS generation, Am J Transl Res 11 (8) (2019) 5008–5018.
[15] I. da Silva Brum, J.J. de Carvalho, J.L. da Silva Pires, et al., Nanosized hydroxyapatite and beta-tricalcium phosphate composite: physico-chemical, cytotoxicity, morphological properties and in vivo trial, Sci. Rep. 9 (1) (2019) 19602.
[16] H. Quan, Y. He, J. Sun, et al., Chemical self-assembly of multifunctional hydroxyapatite with a coral-like nanostructure for osteoporotic bone reconstruction, ACS Appl. Mater. Interfaces 10 (30) (2018) 25547–25560.
[17] Q. Feng, J. Xu, K. Zhang, et al., Dynamic and cell-infiltratable hydrogels as injectable carrier of therapeutic cells and drugs for treating challenging bone defects, ACS Cent. Sci. 5 (3) (2019) 440–450.
[18] S. Lin, G. Yang, F. Jiang, et al., A magnesium-enriched 3D culture system that mimics the bone development microenvironment for vascularized bone regeneration, Adv Sci (Weinh) 6 (12) (2019), 1900209.
[19] W. Liu, J. Li, M. Cheng, et al., Zinc-modified sulfonated polyetheretherketone surface with immunomodulatory function for guiding cell fate and bone regeneration, Adv Sci (Weinh) 5 (10) (2018), 1800749.
[20] B. Brodziak-Dopierala, J. Kwapulinski, K. Sobczyk, D. Wiechula, The content of manganese and iron in hip joint tissue, J. Trace Elem. Med. Biol. 27 (3) (2013) 208–212.
[21] S. Mondal, S. Haldar, P. Saha, T.K. Ghosh, Metabolism and tissue distribution of trace elements in broiler chickens' fed diets containing deficient and plethoric levels of copper, manganese, and zinc, Biol. Trace Elem. Res. 137 (2) (2010) 190–205.
[22] D. Carluccio, C. Xu, J. Venezuela, et al., Additively manufactured iron-manganese for biodegradable porous load-bearing bone scaffold applications, Acta Biomater. 103 (2020) 346–360.
[23] B. Bracci, P. Torricelli, S. Panzavolta, et al., Effect of Mg(2+), Sr(2+), and Mn(2+) on the chemico-physical and in vitro biological properties of calcium phosphate biomimetic coatings, J. Inorg. Biochem. 103 (12) (2009) 1666–1674.
[24] F. Luthen, U. Bulnheim, P.D. Muller, et al., Influence of manganese ions on cellular behavior of human osteoblasts in vitro, Biomol. Eng. 24 (5) (2007) 531–536.
[25] L. Yu, Y. Tian, Y. Qiao, X. Liu, Mn-containing titanium surface with favorable osteogenic and antimicrobial functions synthesized by PIII&D, Colloids Surf. B Biointerfaces 152 (2017) 376–384.
[26] Synthesis, characterisation and antimicrobial activity of manganese- and iron-doped zinc oxide nanoparticles, J. Exp. Nanosci. 11 (1) (2016) 54–71, https://doi.org/10.1080/17458080.2015.1025302.
[27] B.R. Barrioni, E. Norris, S. Li, et al., Osteogenic potential of sol-gel bioactive glasses containing manganese, J. Mater. Sci. Mater. Med. 30 (7) (2019) 86.
[28] Y.J. Bae, M.H. Kim, Manganese supplementation improves mineral density of the spine and femur and serum osteocalcin in rats, Biol. Trace Elem. Res. 124 (1) (2008) 28–34.
[29] P.M. Torres, S.I. Vieira, A.R. Cerqueira, et al., Effects of Mn-doping on the structure and biological properties of beta-tricalcium phosphate, J. Inorg. Biochem. 136 (2014) 57–66.
[30] H. Rico, N. Gomez-Raso, M. Revilla, et al., Effects on bone loss of manganese alone or with copper supplement in ovariectomized rats. A morphometric and densitomeric study, Eur. J. Obstet. Gynecol. Reprod. Biol. 90 (1) (2000) 97–101.
[31] J.M. Li, S.C. Chen, et al., Combined effects of hypoxia and excess Mn2+ on oxidative stress and antioxidant enzymes in tomato seedlings, Russ. J. Plant Physiol. 59 (5) (2012), 670–678(9).
[32] S. Hyeon, H. Lee, Y. Yang, W. Jeong, Nrf2 deficiency induces oxidative stress and promotes RANKL-induced osteoclast differentiation, Free Radic. Biol. Med. 65 (2013) 789–799.
[33] I. Bellezza, I. Giambanco, A. Minelli, R. Donato, Nrf2-Keap1 signaling in oxidative and reductive stress, Biochim. Biophys. Acta Mol. Cell Res. 1865 (5) (2018) 721–733.
[34] M. Zaidi, Skeletal remodeling in health and disease, Nat. Med. 13 (7) (2007) 791–801.
[35] A. Anesi, L. Generali, L. Sandoni, S. Pozzi, A. Grande, From osteoclast differentiation to osteonecrosis of the jaw: molecular and clinical insights, Int. J. Mol. Sci. 20 (19) (2019).
[36] P.D. Miller, Anti-resorptives in the management of osteoporosis, Best Pract. Res. Clin. Endocrinol. Metabol. 22 (5) (2008) 849–868.
[37] P.D. Miller, R.J. Derman, What is the best balance of benefits and risks among anti-resorptive therapies for postmenopausal osteoporosis? Osteoporos. Int. 21 (11) (2010) 1793–1802.
[38] J. Jeong, J.H. Kim, J.H. Shim, N.S. Hwang, C.Y. Heo, Bioactive calcium phosphate materials and applications in bone regeneration, Biomater. Res. 23 (2019) 4.
[39] L. Strause, P. Saltman, J. Glowacki, The effect of deficiencies of manganese and copper on osteoinduction and on resorption of bone particles in rats, Calcif. Tissue Int. 41 (3) (1987) 145–150.
[40] W.L. Ries, L.L. Key Jr., R.M. Rodriguiz, Nitroblue tetrazolium reduction and bone resorption by osteoclasts in vitro inhibited by a manganese-based superoxide dismutase mimic, J. Bone Miner. Res. 7 (8) (1992) 931–939.
[41] G. Zhou, Y. Li, B. Zheng, et al., Cerium oxide nanoparticles protect primary osteoblasts against hydrogen peroxide induced oxidative damage, Micro & Nano Lett. 9 (2) (2014) 91–96.
[42] X. Cao, D. Luo, T. Li, et al., MnTBAP inhibits bone loss in ovariectomized rats by reducing mitochondrial oxidative stress in osteoblasts, J. Bone Miner. Metabol. 38 (1) (2020) 27–37.
[43] S.C. Manolagas, From estrogen-centric to aging and oxidative stress: a revised perspective of the pathogenesis of osteoporosis, Endocr. Rev. 31 (3) (2010) 266–300.
[44] L. Yan, M. Liang, T. Yang, et al., The immunoregulatory role of myeloid-derived suppressor cells in the pathogenesis of rheumatoid arthritis, Front. Immunol. 11 (2020), 568362.
[45] M. Arra, G. Swarnkar, K. Ke, et al., LDHA-mediated ROS generation in chondrocytes is a potential therapeutic target for osteoarthritis, Nat. Commun. 11 (1) (2020) 3427.
[46] W. Tu, H. Wang, S. Li, Q. Liu, H. Sha, The anti-inflammatory and anti-oxidant mechanisms of the keap1/nrf2/ARE signaling pathway in chronic diseases, Aging Dis 10 (3) (2019) 637–651.
[47] Z. Liu, Y. Hou, L. Li, et al., Nrf2 deficiency aggravates the increase in osteoclastogenesis and bone loss induced by inorganic arsenic, Toxicol. Appl. Pharmacol. 367 (2019) 62–70.
[48] D. Thummuri, V.G.M. Naidu, P. Chaudhari, Carnosic acid attenuates RANKL-induced oxidative stress and osteoclastogenesis via induction of Nrf2 and suppression of NF-kappaB and MAPK signalling, J. Mol. Med. (Berl.) 95 (10) (2017) 1065–1076.